Supplementary Materials

Theoretical Understanding of the In-plane Tensile Strain Effects on Enhancing the Ferroelectric Performance of $Hf_{0.5}Zr_{0.5}O_2$ and ZrO_2 Thin Films

Kun Hee Ye[1,2], Taeyoung Jeong[1,2], Seungjae Yoon[1,2], Dohyun Kim[1,2], Cheol Seong Hwang[*,2], and Jung-Hae Choi[*,1]

[1]*Electronic Materials Research Center, Korea Institute of Science and Technology, Seoul 02792, Korea*

[2]*Department of Materials Science and Engineering and Inter-University Semiconductor Research Center, Seoul National University, Seoul 08826, Korea*

**Corresponding author;*

Tel.: +82 2 880 7535. Fax: +82 2 884 1413

E-mail address: cheolsh@snu.ac.kr *(C. S. Hwang)*

Tel.: +82 2 958 5488. Fax: +82 2 958 6658

E-mail address: choijh@kist.re.kr *(J.-H. Choi)*

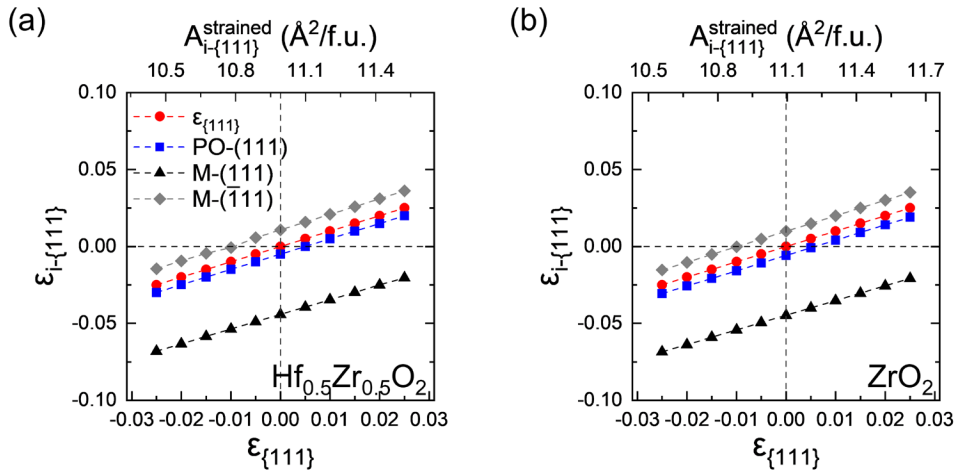

Figure S1. $\varepsilon_{i-\{111\}}$ of the PO-(111) (blue), M-(111) (black), and M-($\bar{1}$11) (gray) as a function of $\varepsilon_{\{111\}}$ (lower x-axis) and $A^{strained}_{i-\{111\}}$ (upper x-axis) in (a) $Hf_{0.5}Zr_{0.5}O_2$ and (b) ZrO_2. $\varepsilon_{i-\{111\}}$ is defined as $\sqrt{\frac{A^{strained}_{i-\{111\}}}{A^{equil}_{i-\{111\}}}} - 1$, where $A^{equil}_{i-\{111\}}$ represents the equilibrium in-plane area of the i-phase. $\varepsilon_{\{111\}} = \sqrt{\frac{A^{strained}_{i-\{111\}}}{A^{equil}_{T-(111)}}} - 1$ is also shown in red as a guide.

Notes for Figure S1: Due to the discrepancies in lattice parameters and consequent $A^{equil}_{i-\{111\}}$ among polymorphs in Table I, $\varepsilon_{i-\{111\}}$ values also differ among polymorphs for a given $A^{strained}_{i-\{111\}}$ and $\varepsilon_{\{111\}}$. In $Hf_{0.5}Zr_{0.5}O_2$, for instance, $\varepsilon_{M-(111)}$ is always negative, indicating the M-(111) undergoes the in-plane compressive strain compared to the M-phase in equilibrium for all $\varepsilon_{\{111\}}$ range investigated. On the other hand, the M-($\bar{1}$11) is under in-plane tensile strain (i. e., positive $\varepsilon_{M-(\bar{1}11)}$) at $\varepsilon_{\{111\}} > -0.005$, while under in-plane compressive strain (i. e., negative $\varepsilon_{M-(\bar{1}11)}$) at $\varepsilon_{\{111\}} < -0.01$ compared to the M-phase in equilibrium.

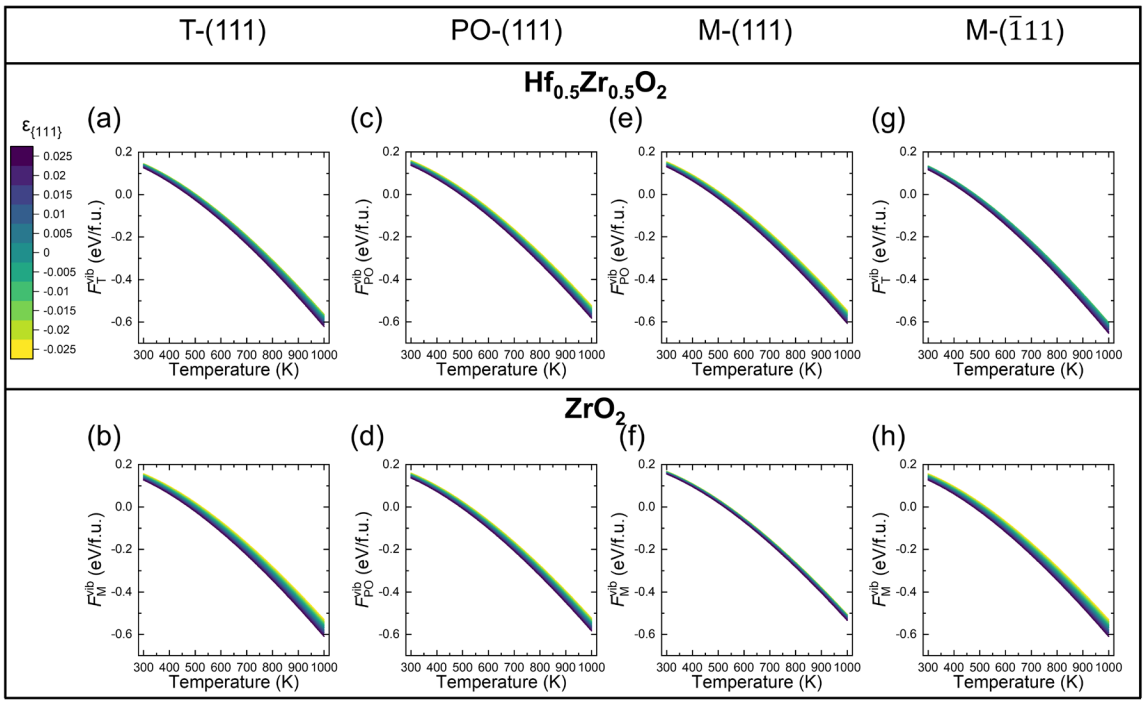

Figure S2. F_i^{vib} of (a,b) T-(111), (c,d) PO-(111), (e,f) M-(111), and (g,h) M-($\bar{1}11$) depending on temperature in (a,c,e,g) $Hf_{0.5}Zr_{0.5}O_2$ and (b,d,f,h) ZrO_2. The color bar represents the scale of $\varepsilon_{\{111\}}$.

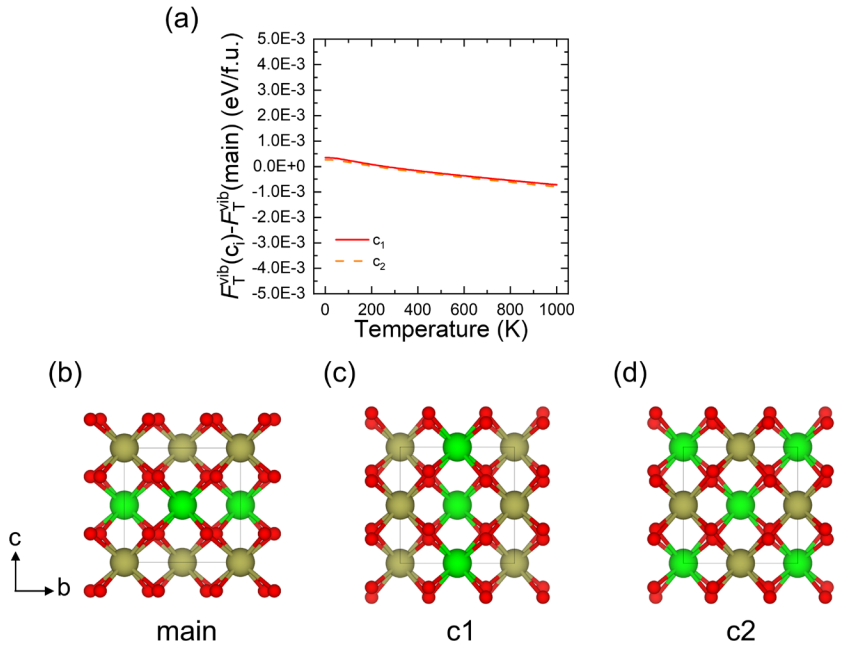

Figure S3. (a) Temperature- and configuration-dependent F_T^{vib} of the T-phase $Hf_{0.5}Zr_{0.5}O_2$. The cation configurations of the T-phase $Hf_{0.5}Zr_{0.5}O_2$ are represented in (b~d).

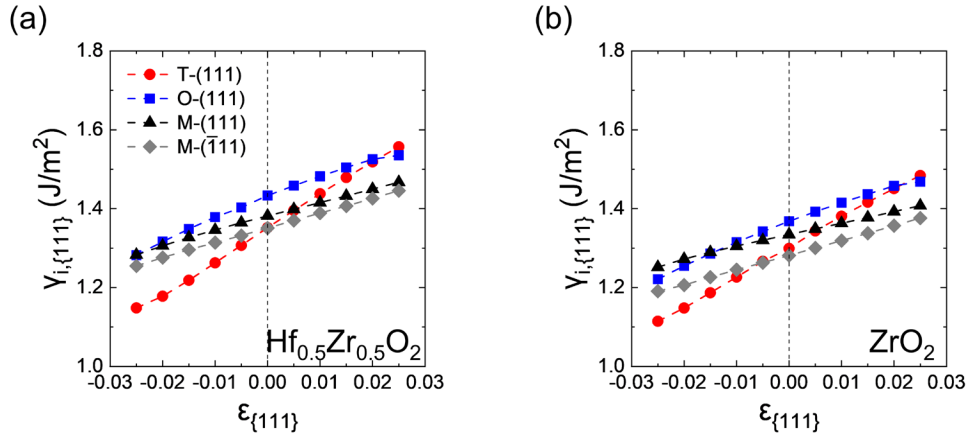

Figure S4. $\gamma_{i,\{111\}}$ of T-(111), O-(111), M-(111), and M-($\bar{1}$11) depending on $\varepsilon_{\{111\}}$ in (a) $Hf_{0.5}Zr_{0.5}O_2$ and (b) ZrO_2. The O-(111) represents the (111) plane of the antipolar orthorhombic structure.

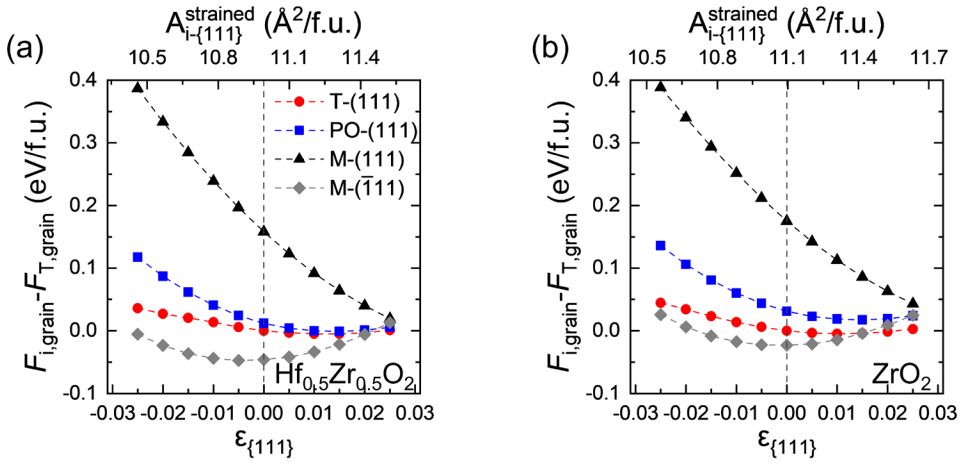

Figure S5. $F_{i,grain}$ at 1000 K for the T-(111), PO-(111), M-(111), and M-($\bar{1}$11) grains as a function of $\varepsilon_{\{111\}}$ (lower x-axis) and $A^{strained}_{i-\{111\}}$ (upper x-axis) in (a) $Hf_{0.5}Zr_{0.5}O_2$ and (b) ZrO_2.

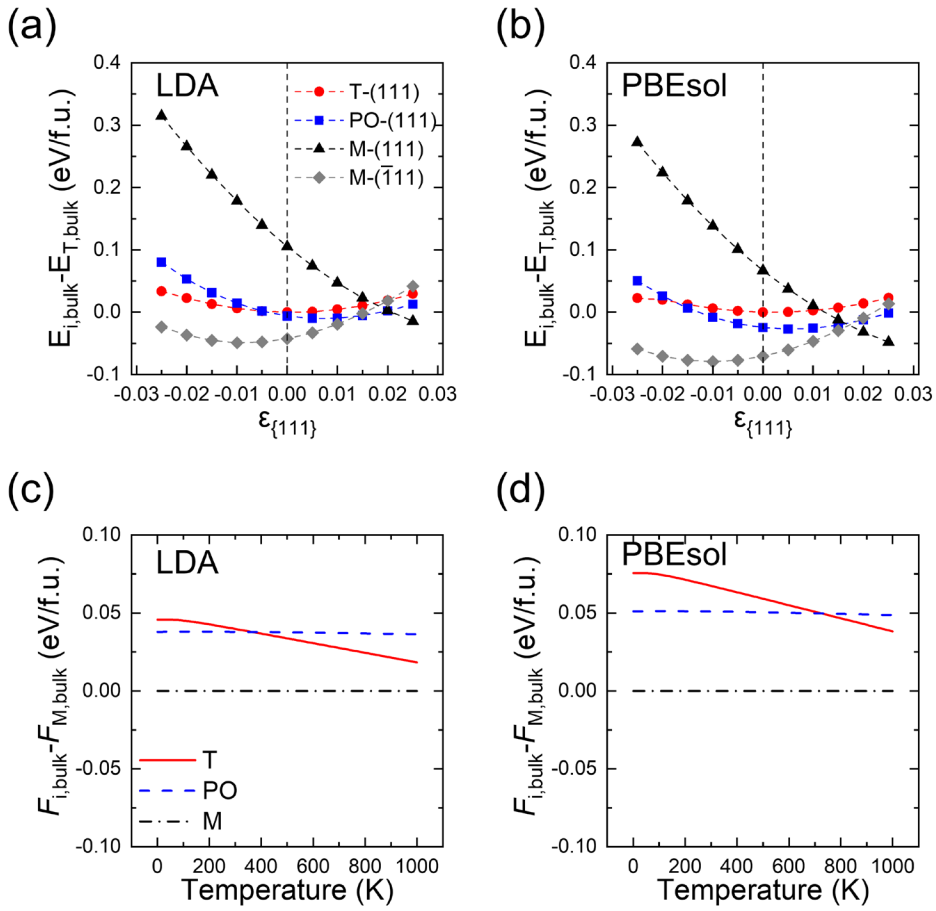

Figure S6. (a,b) $\varepsilon_{\{111\}}$-dependent $E_{i,bulk}$ of ZrO_2 calculated by (a) LDA and (b) PBEsol functionals. (c,d) Temperature-dependent $F_{i,bulk}$ of ZrO_2 calculated by (c) LDA and (d) PBEsol functionals.

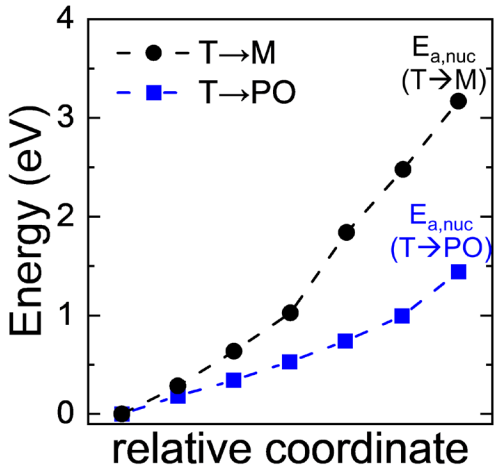

Figure S7. Energy profiles during the nucleation of a single unitcell of M- and PO-phases in 3×3×3 T-phase supercell using the nudged elastic band method.

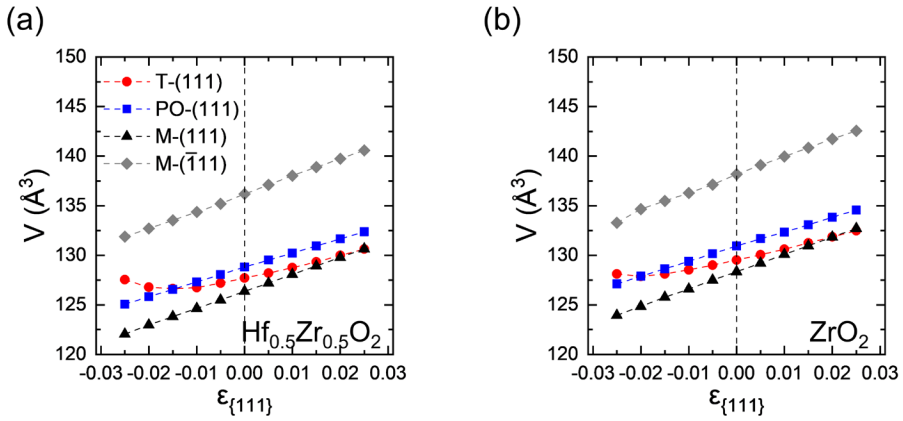

Figure S8. Conventional unit cell volume of the T-(111), PO-(111), M-(111), and M-($\bar{1}$11) grains depending on $\varepsilon_{\{111\}}$ in (a) $Hf_{0.5}Zr_{0.5}O_2$ and (b) ZrO_2.

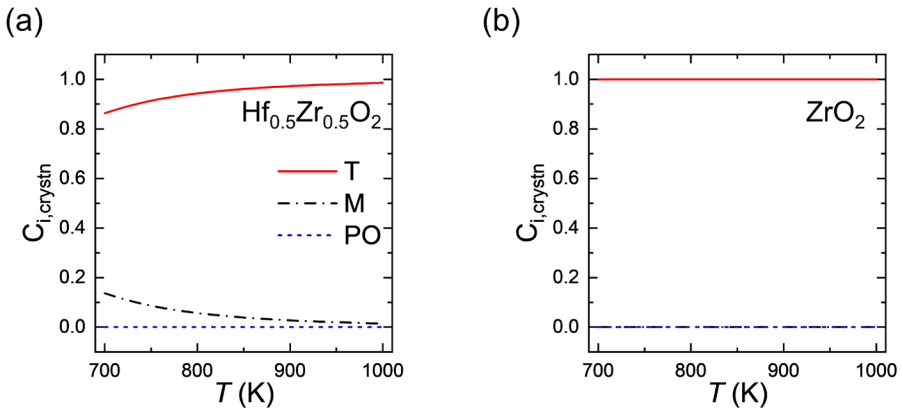

Figure S9. *T*-dependent phase fraction of the T-, M-, and PO-phases crystallized from amorphous ($C_{T,crystn}$, $C_{M,crystn}$, and $C_{PO,crystn}$) in (a) $Hf_{0.5}Zr_{0.5}O_2$ and (b) ZrO_2.

Notes for Figure S9: The crystallization rate, $R_{i,crystn}$, was calculated as;

$$R_{\mathrm{i,crystn}} = N_s \nu_0 \exp\left(\frac{-\Delta F_{\mathrm{i}}^*}{k_B T_{\mathrm{crystn}}}\right)$$

, where the ΔF_{i}^* is the crystallization barrier of the i-phase described in the previous study [1]. The differences in pre-exponential factors of N_s (the number of nucleation sites) and ν_0 among polymorphs were assumed to be negligible. Using the $R_{i,crystn}$, $C_{i,crystn}$ was calculated by the following equation.

$$\mathrm{C_{i,crystn}} = \frac{R_{\mathrm{i,crystn}}}{R_{\mathrm{M,crystn}} + R_{\mathrm{T,crystn}} + R_{\mathrm{PO,crystn}}}$$

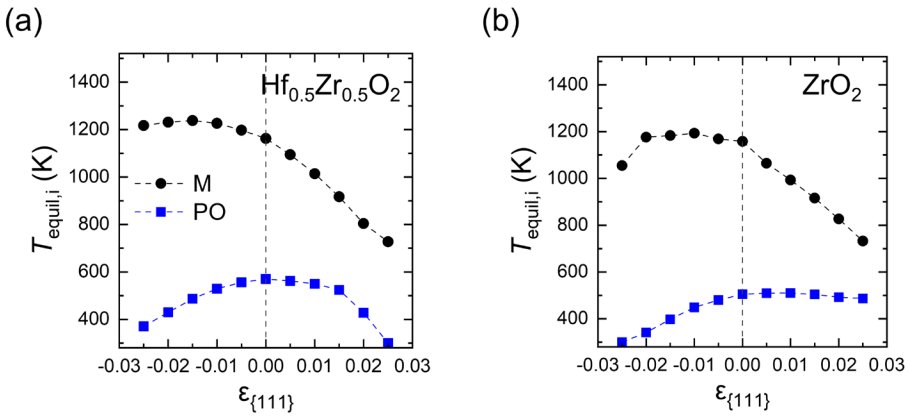

Figure S10. $\varepsilon_{\{111\}}$ -dependent equilibrium temperatures of M- and PO-phases ($T_{equil,M}$ and $T_{equil,PO}$) in (a) $Hf_{0.5}Zr_{0.5}O_2$ and (b) ZrO_2.

References

[1] K.H. Ye, I.W. Yeu, G. Han, T. Jeong, S. Yoon, D. Kim, C.S. Hwang, and J.H. Choi, "Comprehensive interpretations of thermodynamic and kinetic effects on the phase fractions in $Hf_{1-x}Zr_xO_2$ by first principle calculations," *Appl. Phys. Rev.* **10**, 031419 (2023).